Elastic, inelastic, and 1*n* transfer cross sections for the ^{10}B + ^{120}Sn reaction

L. R. Gasques, A. S. Freitas, L. C. Chamon, J. R. B. Oliveira, N. H. Medina, V. Scarduelli, and E. S. Rossi Jr.
Instituto de Física da Universidade de São Paulo, 05508-090, São Paulo, SP, Brazil

M. A. G. Alvarez
Departamento FAMN, Universidad de Sevilla, Apartado 1065, 41080 Sevilla, Spain

V. A. B. Zagatto and J. Lubian
Instituto de Física da Universidade Federal Fluminense, 24210-346, Niterói, Rio de Janeiro, Brazil

G. P. A. Nobre
National Nuclear Data Center, Brookhaven National Laboratory, Upton, New York 11973-5000, USA

I. Padron
Centro de Aplicaciones Tecnológicas y Desarrollo Nuclear, 502, Calle 30, La Habana, Cuba

B. V. Carlson
Departamento de Física, Instituto Tecnológico de Aeronáutica, Centro Técnico Aeroespacial, São José dos Campos, SP, Brazil

(Received 30 November 2017; published 30 March 2018)

The ^{10}B + ^{120}Sn reaction has been investigated at $E_{\rm Lab} = 37.5$ MeV. The cross sections for different channels, such as the elastic scattering, the excitation of the 2^+ and 3^- ^{120}Sn states, the excitation of the 1^+ state of ^{10}B, and the 1*n* pick-up transfer, have been measured. One-step distorted-wave Born approximation and coupled-reaction-channels calculations have been performed in the context of the double-folding São Paulo potential. The effect of coupling the inelastic and transfer states on the angular distributions is discussed in the paper. In general, the theoretical calculations within the coupled-reaction-channels formalism yield a satisfactory agreement with the corresponding experimental angular distributions.

DOI: 10.1103/PhysRevC.97.034629

I. INTRODUCTION

Since Rutherford's famous experiment [1] performed in the beginning of the 1900s, which has demonstrated that almost the entire mass of an atom is concentrated in its nucleus, many important discoveries have been made in the field of nuclear structure and reactions. In particular, in the 1980s, Tanihata and collaborators have observed a significant increase of the radii of the ^{6,8}He and ^{11}Li nuclei [2,3]. A few years later, Hansen and Jonson introduced the term "halo" to refer to these nuclei, formed by a strongly bound core and one or two valence nucleons [4]. Since then, numerous scientific works have been published, exploring important properties about the structure of nuclei far from the valley of stability. The possibility of producing nuclei rich in protons and neutrons has opened new frontiers in the field of physics and nuclear astrophysics, encouraging the study of innumerable reactions involving weakly bound and exotic nuclei [5–9]. Such studies are continually performed in several laboratories and research centers around the world.

Despite the many advances made since the first accelerator was built, the production of radioactive beams with intensities comparable to those typical of stable nuclei still represents a major technological challenge. In general, beams of exotic nuclei are produced with intensities ranging from 10^4 to 10^7 particles per second. While radioactive beams are not produced at sufficiently high intensities, the study of reactions involving stable weakly bound projectiles, such as ^{6,7}Li, ^{9}Be, and ^{10}B, represents an interesting alternative. Weakly bound nuclei are very likely to undergo a break-up process during interaction with the target nucleus, giving rise to a complex problem of three or more bodies. In the past few decades, collisions involving stable weakly bound nuclei have been extensively studied at energies around the Coulomb barrier, as they represent an important tool to observe and disentagle competing reaction mechanisms [10–14]. Recent results have clearly demonstrated that, in collisions involving weakly bound projectiles, break-up may occur by two different modes: the process can be associated to the direct excitation of weakly bound projectiles into continuum states, or it can occur populating unbound excited states of a projectile-like nucleus following nucleon transfer [15–17]. In nuclear astrophysics, Coulomb break up of weakly bound projectiles has been used as an indirect method for determining cross sections of radiative capture processes [18–20].

Within this context, we intend to perform a systematic study involving the scattering of weakly bound projectiles impinging on ^{120}Sn. In fact, we have already measured angular distributions for the ^{7}Li + ^{120}Sn reaction at energies around the

barrier [21]. In Ref. [13], fusion cross sections were reported for the ^{10,11}B + ^{209}Bi reactions. It was shown that the weak binding energy of ^{10}B, compared with ^{11}B, results in a larger suppression factor for the fusion cross sections at energies above the Coulomb barrier. In the present paper, we report on the study of the reaction mechanisms of ^{10}B impinging on an ^{120}Sn target. We have measured the elastic-scattering angular distribution at 37.5 MeV beam energy, which is about 2 MeV above the Coulomb barrier height. In addition to elastic scattering, other channels have been observed, such as the excitation of the 2^+ and 3^- ^{120}Sn states and of the 1^+ ^{10}B first excited state and the $1n$ pick-up transfer. The corresponding cross sections have been experimentally determined, and the results compared with theoretical calculations performed within the one-step distorted-wave Born approximation (DWBA) and coupled-reaction-channels (CRC) formalisms.

The paper is organized as follows: The experimental setup is briefly described in Sec. II, experimental results are compared with theoretical predictions in Sec. III, and the main conclusions are presented in Sec. IV.

II. EXPERIMENTAL SETUP

The experiment was performed at the Institute of Physics of the University of São Paulo (USP), using the Pelletron accelerator installed in the Open Laboratory of Nuclear Physics (LAFN, acronym in Portuguese). The beam was produced from an isotopically enriched ^{10}B cathode mounted in the SNICS ion source and delivered to the 30B beamline of the LAFN with 4^+ charge state. Typical beam intensities of about 75 particle nanoampere on the ^{120}Sn target were obtained during the experiment. The bombarding energy was 37.5 MeV. The targets were made through thin isotopically enriched (>99%) foils of ^{120}Sn, with thickness around 100 μg/cm^2. A thin backing layer of ^{197}Au was evaporated in the targets for normalization purposes, since at this energy the corresponding elastic-scattering cross section is associated to the Rutherford one.

The experimental arrangement was similar to that reported in Ref. [21], and only a brief description is given here. The Silicon Array and Telescopes of Usp for Reactions and Nuclear applications (SATURN) system was used in the experiment. With this detecting system, it is possible to mount up to nine surface barrier detectors in angular intervals of 5°. The SATURN system is fixed on a rotating wheel, allowing changes in the detector angular positions without breaking the vacuum of the scattering chamber. For each detector, an energy calibration was performed using the elastic-scattering peaks of ^{10}B incident on ^{120}Sn and ^{197}Au targets. For illustration, a typical spectrum taken at $\theta_{\rm Lab} = 125°$ is shown in Fig. 1. All the peaks have been identified and labeled using different colors. The elastic-scattering peak of ^{10}B incident on ^{120}Sn is labeled in orange. The peaks corresponding to the different excited states energy in ^{119}Sn populated following $1n$ transfer are indicated by the blue arrows. The 1^+ ^{10}B first excited state is given in red, while the excitation of the 2^+ and 3^- ^{120}Sn states are indicated by the green arrows.

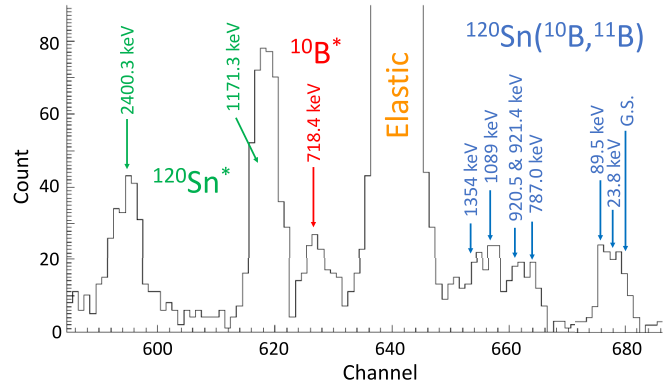

FIG. 1. Spectrum taken at $\theta_{\rm Lab} = 125°$. The peaks corresponding to the $1n$ pick-up transfer (blue), elastic scattering of ^{10}B on ^{120}Sn target (orange), 1^+ ^{10}B first excited state (red), and the excitation of the 2^+ (1173 keV) and 3^- (2400 keV) ^{120}Sn states (green) can be clearly identified in the figure.

III. DATA ANALYSIS AND RESULTS

Differential cross sections for the elastic, inelastic, and $1n$ pick-up channels have been experimentally determined through the corresponding yields observed in the spectra. In the case of the $1n$ pick-up transfer, peaks corresponding to different neighboring states of the compound ^{119}Sn nucleus are situated in two relatively broad groups in the spectra. Therefore, the two $1n$ pick-up angular distributions presented in this paper correspond to the sum of the cross sections of close-by-populated excited states of the residual ^{119}Sn nucleus. In fact, the yield of higher level excited states of ^{119}Sn or ^{11}B could provide some contribution at the same region of elastic and inelastic peaks. Therefore, the cross sections for the inelastic channels could be slightly overestimated in the present work.

Aiming for a simultaneous description of these channels, we have performed CRC calculations assuming the double-folding São Paulo potential (SPP) for the real part of the nuclear interaction [22]. In order to study the effect of the couplings on the different channels, we have compared the CRC cross sections with those obtained from DWBA calculations. In both cases, the imaginary part assumed for the optical potential was calculated by summing two terms, one of them is restricted to the internal region of the barrier radius and another extending to the surface region. The first is represented by a Woods-Saxon short-ranged potential, given by $W_0 = 100.0$ MeV, $r_0 = 0.8$ fm, and $a = 0.25$ fm, while the second is obtained multiplying the SPP by a given normalization factor (N_i). The contribution of the Woods-Saxon term is important only to warrant an internal absorption of flux from the elastic channel when N_i is set to zero.

The FRESCO code [23] was used to calculate the theoretical cross sections. A collective vibrational mode was assumed to describe the excited states of the ^{120}Sn, whereas the ^{10}B was treated through two alternatives: as a rotor and as a vibrational nucleus. Within these two assumptions, the overall description of the experimental data is quite similar. Therefore, spin

TABLE I. Spin, excitation energies (MeV), transition amplitudes from the ground state to the excited states (e^2b^λ), and deformation lengths (fm) for the states included in the CRC calculations.

Nucleus	Spin	E^*	λ	$B(E\lambda)\uparrow$	δ_λ
^{10}B	1^+	0.718	2	3.3×10^{-4}	0.90
^{120}Sn	2^+	1.171	2	0.25	0.80
^{120}Sn	3^-	2.400	3	0.10	0.79

reorientation effects of the projectile have minor significance on the reaction mechanisms. In what follows we only show the results obtained with the rotational model (for ^{10}B).

A. CRC calculations

CRC calculations were performed by including 3 states related to the inelastic excitations of projectile and target, 8 states related to the one-neutron transfer [^{120}Sn(^{10}B,^{11}B)^{119}Sn], and 13 states of one-proton transfer [^{120}Sn(^{10}B,^{9}Be)^{121}Sb]. Although not observed in our spectra, we included the 1p transfer in our CRC calculations only to verify its possible effect on the other channels. However, the effect of couplings associated to the 1n and 1p transfer channels on the elastic and inelastic cross sections is negligible.

In this section we focus our discussion only on the elastic and inelastic angular distribution data. Subsequently, in a separated section, we present a discussion about the transfer cross sections.

For the ^{120}Sn Coulomb transition amplitudes, $B(E2;0^+\rightarrow 2^+)$ and $B(E2;0^+\rightarrow 3^+)$, we have adopted the values reported in Refs. [24,25]. For the case of the quadrupole transition in ^{10}B, the value of $B(E2;3^+\rightarrow 1^+)=1.79\times10^{-4}\ e^2\ \mathrm{b}^2$ quoted in literature [26] does not give a satisfactory description of the experimental cross section for the inelastic excitation of the 1^+ state in the forward angular region. In order to amend this discrepancy, we have adjusted the $B(E2)$ parameter and obtained a value which is about twice that of Ref. [26]. The nuclear deformation parameters δ_λ of projectile and target were calculated from the respective $B(E2)$ and $B(E3)$ values taking into account the effect of the finite diffuseness value of the nuclear density, as described in Refs. [25,27]. Adopting this procedure, the values of δ_λ become smaller than those determined from the sharp cut-off model. Table I lists the spin of projectile and target excited states considered in the coupling scheme, along with the corresponding transition mode, excitation energy, Coulomb transition probability, and deformation length.

The experimental elastic-scattering angular distribution measured at $E_{\mathrm{Lab}}=37.5$ MeV is presented in Fig. 2. The statistical error bars of the elastic-scattering cross sections vary from 0.6% to 2.5% over the entire angular range. The figure also show the results of the CRC calculations assuming the SPP for the real part of the optical potential. The curves correspond to different N_i values (for the imaginary potential). Even though none of the curves results in a remarkable agreement with the data, assuming $N_i=0.25$ allows a reasonable description of the elastic cross sections throughout the whole angular range. Despite the relatively large number of states coupled to the entrance channel, the theoretical cross sections do not reproduce the data around the Fresnel region ($\theta_{\mathrm{c.m.}}\sim 85^\circ$). As ^{10}B is a weakly bound nucleus, it may break up into a number of different mass partitions, being the most energetically favorable the $^{10}\mathrm{B}\rightarrow{}^{6}\mathrm{Li}+{}^{4}\mathrm{He}$ ($Q=-4.461$ MeV). In the case of ^{7}Li + ^{120}Sn, the inclusion of the effect of the breakup results in a slightly better description of the data [21]. Therefore, for the ^{10}B + ^{120}Sn, it may be necessary to include couplings to continuum states to improve the agreement between theory and experiment. Such calculations are beyond the scope of the present work.

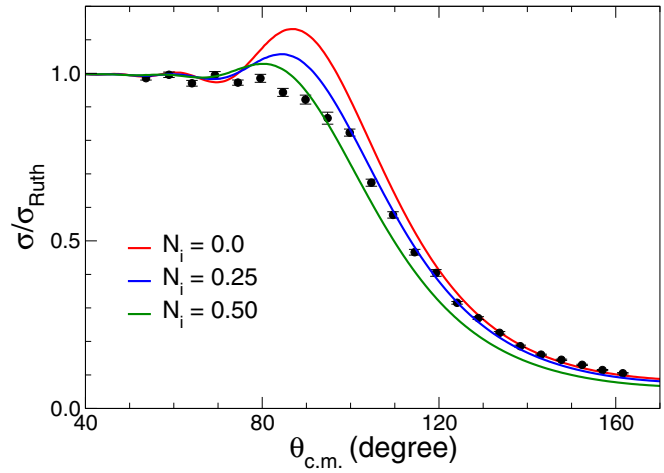

FIG. 2. Experimental cross sections and CRC results for the elastic-scattering angular distribution of ^{10}B + ^{120}Sn at 37.5 MeV bombarding energy. The curves were obtained using different values for the normalization factor of the imaginary part of the optical potential.

Figure 3 presents the cross sections for the inelastic excitation of the ^{10}B (1^+, 0.718 MeV) state. The cross sections

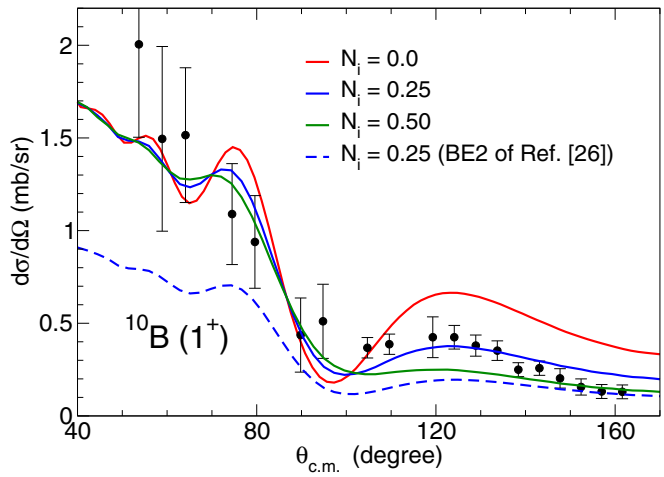

FIG. 3. Inelastic-scattering angular distribution for the quadrupole excitation in ^{10}B. The theoretical curves were obtained using different values for the normalization factor of the imaginary part of the optical potential. The dashed line corresponds to the results obtained with the $B(E2)$ value of Ref. [26].

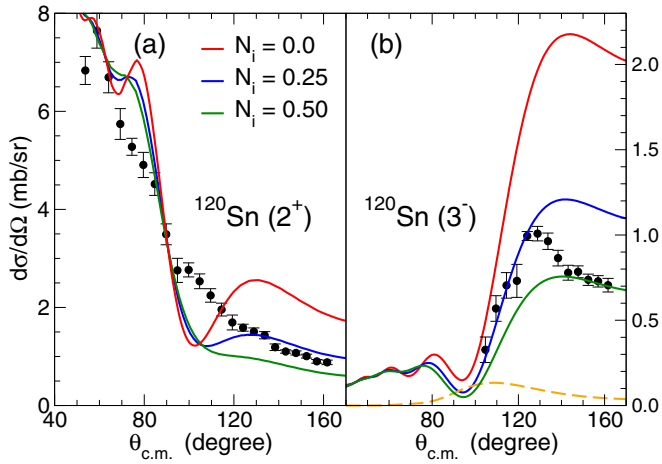

FIG. 4. Inelastic-scattering angular distributions for (a) quadrupole and (b) octupole excitations in ^{120}Sn. The theoretical curves were obtained using different values for the normalization factor of the imaginary part of the optical potential. The dashed orange curve in panel (b) corresponds to the $1n$ transfer cross section forming the $5/2^-$ ^{11}B state (4.45 MeV of excitation energy).

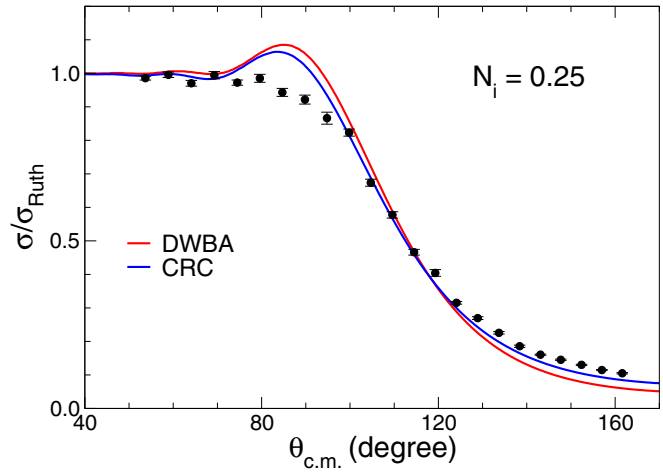

FIG. 5. Experimental elastic-scattering angular distribution for ^{10}B + ^{120}Sn at 37.5 MeV. The curves represent the results of DWBA and CRC calculations, using $N_i = 0.25$ for the imaginary part of the optical potential.

corresponding to the inelastic excitations of the ^{120}Sn (2^+, 1.171 MeV and 3^-, 2.400 MeV) are shown in Fig. 4. The curves presented in these figures are the results of CRC calculations. The theoretical cross sections obtained by adopting an imaginary potential only with internal absorption ($N_i = 0$) overpredict the experimental data at backward angles, where the collision dynamics is largely dominated by the nuclear interaction. At forward angles, that corresponds to the region in which the Coulomb interaction dominates, the calculated cross sections are barely sensitive to the N_i values. Once more, the best CRC results are obtained by assuming $N_i = 0.25$.

The dashed blue line in Fig. 3 represents the results obtained for the inelastic excitation of the ^{10}B (1^+, 0.718 MeV) state, where the value $B(E2; 3^+ \rightarrow 1^+) = 1.79 \times 10^{-4}\ e^2\text{b}^2$ of Ref. [26] was assumed. Clearly, there is a disagreement between data and theoretical cross sections. Even at the forward angular region, that is not sensitive to changes in the N_i value, the data are about twice larger than the theoretical cross sections. Part of this discrepancy might be related to a possible contribution to the inelastic data arising from some contamination due to the $1n$ transfer process populating high excited states of ^{119}Sn.

Measurements of angular distributions for the $^{10}\text{B}(d,p)^{11}\text{B}$ reaction have shown a strong population of the $5/2^-$ ^{11}B state with 4.45 MeV of excitation energy [28]. In the present work, the yields arising from this process lie in the same region of the spectra as the inelastic channel corresponding to the 3^- ^{120}Sn state (2.400 MeV). In order to estimate the contribution of the $5/2^-$ $1n$ transfer channel on the 3^- inelastic yields, we have calculated the corresponding $1n$ transfer cross sections. The CRC calculations have been performed using $N_i = 0.25$ for the imaginary potential. Following the results presented in Ref. [28], the respective spectroscopic factor ($\text{C}^2\text{S} = 0.34$) was calculated as about one third of the spectroscopic factor associated to the ground-state transition for the overlap $\langle ^{11}\text{B} \mid ^{10}\text{B} + \text{n}\rangle$ (obtained in Ref. [29]). The results are shown in Fig. 4 (dashed orange curve). As can be seen, at scattering angles around 105°, the $1n$ cross section reaches its maximum value. At this region, a comparison between the blue and orange curves reveal that the inelastic cross sections are about 3 times larger than the $1n$ transfer ones. Therefore, any possible contribution of the $5/2^-$ ^{11}B state related to the $1n$ transfer would marginally affect the data corresponding to the 3^- ^{120}Sn inelastic process.

B. One-step DWBA calculations

The DWBA formalism has been extensively used to study direct reaction mechanisms in collisions of heavy-ion nuclei. In the present paper, we have employed this formalism to obtain elastic- and inelastic-scattering angular distributions, as well as cross sections for the $1n$ pick-up transfer. Adopting the DWBA formalism, the cross section of a particular reaction channel is not modified by the couplings with other channels. Therefore, the comparison of such theoretical results with CRC cross sections and experimental data is important to investigate whether the couplings are relevant for the description of the main reaction channels.

The results for the elastic-scattering angular distribution at 37.5 MeV are shown in Fig. 5. The red and blue solid lines in this figure are the results of DWBA and CRC calculations, respectively. For the imaginary part of the optical potential, we have adopted $N_i = 0.25$. The direct comparison of the two curves provides the effect of the couplings on the elastic-scattering channel. Although the effect of the couplings is not pronounced, the calculation performed within the CRC formalism gives a better description of the elastic-scattering data in the entire angular region.

Figures 6 and 7 compare the theoretical results obtained with the DWBA and CRC formalisms for the ^{10}B (1^+, 0.718 MeV) and ^{120}Sn (2^+ 1.171 MeV and 3^- 2.400 MeV) inelastic channels, respectively. As can be seen in these figures,

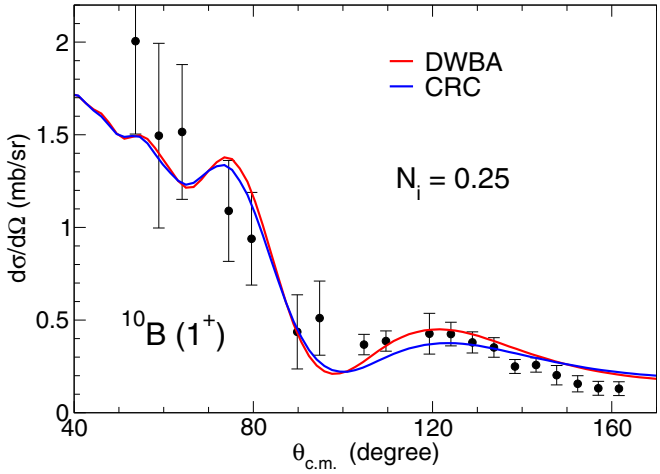

FIG. 6. Inelastic-scattering angular distribution for the excitation of the 1^+ state in ^{10}B. The curves represent the results of the DWBA and CRC calculations, using $N_i = 0.25$ for the imaginary part of the optical potential.

the couplings of a relatively large number of states slightly modify the cross sections mainly at backward angles. In fact, both formalisms provide rather similar results.

C. One-neutron transfer cross sections

The experimental differential cross sections for the 1n pick up, ^{120}Sn(^{10}B,^{11}B)^{119}Sn, corresponding to the ground-state (ground state) Q value of 2.350 MeV, have been determined from the yields of two sets of peaks associated with different excitation energies of the residual ^{119}Sn nucleus. The first set corresponds to the combination of the ground state along with the 23.8- and 89.5-keV energy levels of ^{119}Sn. The second set is formed by the sum of the 787.0-, 920.5-, 921.4-, 1089-, and 1354-keV excited states of the ^{119}Sn residual nucleus.

Figure 8 presents experimental and theoretical (CRC and DWBA) transfer cross sections for the two groups of levels described above. Again the DWBA and CRC theoretical results are quite similar. Although the prescription for dealing with

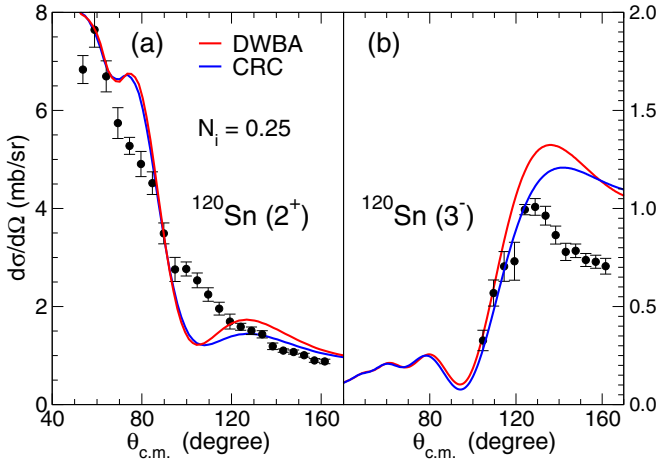

FIG. 7. The same as in Fig. 6 for the 2^+ and 3^- states of ^{120}Sn.

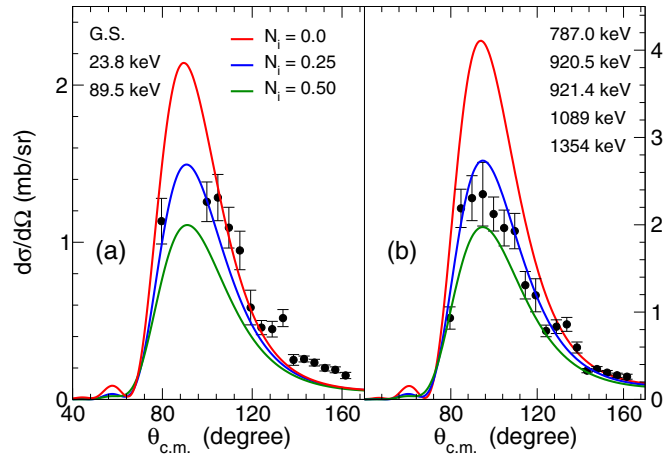

FIG. 8. Comparison between theoretical (CRC and DWBA) and experimental cross sections for the 1n transfer channel. The solid lines represent sums of contributions of two groups of neighboring states of the compound ^{119}Sn nucleus, which were not experimentally resolved.

the transfer calculations is well known, there are many ambiguities when obtaining theoretical cross sections. In the next paragraph, we describe under what conditions the theoretical angular distributions of Fig. 8 were obtained. After that, we discuss the ambiguities found in the calculation of the transfer cross sections.

For the neutron-core potentials, n + ^{10}B and n + ^{119}Sn, we have assumed the Woods-Saxon shape, with radius and diffuseness values presented in Table II. The FRESCO code automatically adjusts the corresponding depth in order to reproduce the respective binding energy of the neutron in the compound system (for each state included in the CRC and DWBA calculations). The V_0 values obtained for the ground state (of ^{11}B and ^{120}Sn) are also provided in Table II (similar values were obtained for the other states). As a general result, the inclusion of a spin-orbit potential to describe the bound states has a negligible effect on the theoretical angular distributions for the transfer process. The optical potential for the entrance channel was also assumed for the outgoing ones, with $N_I = 0.25$. The spectroscopic factor associated to the ground-state transition for the overlap $\langle ^{11}\mathrm{B} \mid ^{10}\mathrm{B} + \mathrm{n}\rangle$ was taken as 1.0943 (according to Ref. [29]). The values for the spectroscopic factors of several states related to the overlap

TABLE II. Parameter values of the Woods-Saxon potentials assumed for the neutron-core systems of the CRC and DWBA transfer calculations. The V_0 values presented in the table provide the right results for the binding energy of one neutron when the compound system is in its ground state (similar values were obtained for the other states).

Composite system	V_0 (MeV)	R_0 (fm)	a (fm)
n+^{10}B	44.4	3.10	0.61
n+^{119}Sn	48.7	6.16	0.65

TABLE III. Level structure of the ^{119}Sn along with the spectroscopic factors for the overlap $\langle ^{120}\mathrm{Sn} \mid ^{119}\mathrm{Sn} + \mathrm{n}\rangle$.

E_x (keV)	State $(n\ell j)$	$C^2S_{\ell j}$
0.0	$3s_{1/2}$	0.58
23.8	$2d_{3/2}$	1.66
89.5	$1h_{11/2}$	3.35
787.0	$1g_{7/2}$	5.15
920.5	$2d_{3/2}$	0.35
921.4	$2d_{5/2}$	0.30
1089	$2d_{5/2}$	2.82
1354	$2d_{5/2}$	0.98

$\langle ^{120}\mathrm{Sn} \mid ^{119}\mathrm{Sn} + \mathrm{n}\rangle$ were obtained through averages over values presented in Ref. [30] (the present values are listed in Table III). For consistency, the radius and diffuseness values that we have assumed for the potential of n + ^{119}Sn are the same as those reported in the paper where the spectroscopic factors were obtained.

To calculate transfer cross sections in the present case, it is necessary to assume models for the nuclear interactions between the neutron with the ^{10}B and ^{119}Sn core nuclei. Apart from the choice of n-core interaction discussed above, another important ingredient involved in the calculations of transfer cross sections is the set of values assumed for the spectroscopic factors associated to the coupled states. As we will see, the transfer cross sections are very sensitive to the adopted geometry for the potential as well as to the values assumed for the spectroscopic factors. Almost identical theoretical angular distributions are obtained within CRC (or DWBA) when assuming different particular sets of values for the parameters involved in such calculations.

There are families of potentials that provide equal values for the binding energy of a given state. For instance, in Figs. 9(c) and 9(d), we present different potentials for n + ^{10}B (ground state) and n + ^{119}Sn (ground state), respectively,

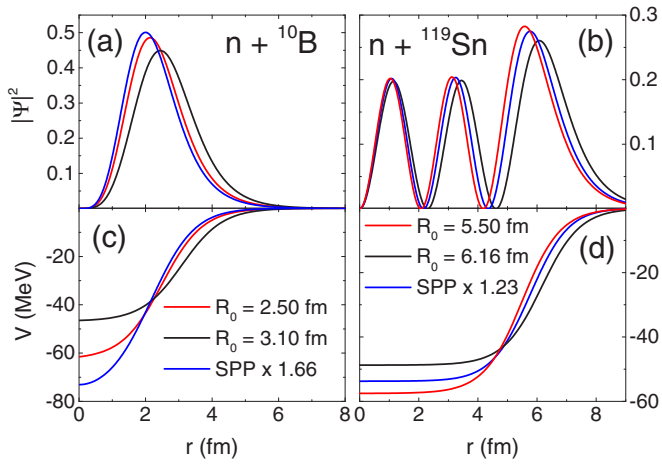

FIG. 9. Wave functions for the (a) n + ^{10}B and (b) n + ^{119}Sn compound systems, together with binding potentials for the (c) n + ^{10}B and (d) n + ^{119}Sn compound systems.

that reproduce the respective one neutron binding energies. For ^{10}B, the figure shows two Woods-Saxon potentials with different radii (the diffuseness is fixed at 0.61 fm) and also the SPP renormalized by a factor 1.66 (the SPP with unitary normalization does not reproduce the binding energy). For n + ^{119}Sn, the SPP must be renormalized by 1.23 to obtain the right value for the neutron binding energy. Since different sets of values for the depth, radius, and diffuseness may be assumed, the parameters of the binding potentials are rather arbitrary. The SPP represents a realistic interaction often assumed to describe scattering data for a large variety of projectile-target combinations. However, as already mentioned, it is necessary to renormalize the SPP to reproduce the binding energy of the n + ^{10}B and n + ^{119}Sn compound systems (for the ground state and excited states). The real part of the potentials obtained from the Koning-Delaroche [31] global systematics (for nucleon-nucleus scattering) could also be assumed for the calculations of bound states. The corresponding depths of such potentials are around 40 MeV. However, we have verified that even in this case a significant renormalization factor is necessary to reproduce the binding energies.

As illustrated in Figs. 9(a) and 9(b), depending on the choice of the R_0 value, the corresponding bound-state wave function associated to the binding potential assume different forms. Larger values for the radius of the potential result in wave functions with a larger spatial extent at the surface region, which favors the transfer process. Therefore, the choice of the values of the parameters related to the potential will impact on the derived values of spectroscopic factors extracted from the transfer cross-section data analyses. In order to illustrate this point, we have varied the value of R_0 associated (only) to n + ^{10}B (keeping the value of the diffuseness fixed), in small steps around 3.0 fm. For each particular R_0 value, the Woods-Saxon depth potential was set in order to reproduce the known binding energy of the ^{11}B ground state. Then, we have found a corresponding spectroscopic factor value (for this state) that result in angular distributions for one neutron transfer with same shape and magnitude that fits the data. The V_0 and spectroscopic factors obtained with this procedure are represented in Fig. 10 as a function of R_0. As can be seen, depending on the choice of the nuclear radius, the spectroscopic factors may vary by a factor as large as 4. Of course, similar ambiguities are also related to the potentials and spectroscopic factors associated to n + ^{119}Sn.

IV. DISCUSSION AND SUMMARY

Elastic, inelastic, and $1n$ transfer angular distributions for ^{10}B + ^{120}Sn have been measured at 37.5 MeV bombarding energy. A simultaneous analysis of the corresponding cross sections has been performed using the CRC and one-step DWBA formalisms, assuming the double-folding SPP for the real part of the nuclear interaction. The imaginary potential was obtained as the sum of two terms. The first was a short-ranged potential of Woods-Saxon shape. The second term was obtained by multiplying the real potential by a certain normalization factor (N_i).

The transition amplitudes $B(E2)$ and $B(E3)$ for excitation of the ^{120}Sn target turned out to be consistent with existing

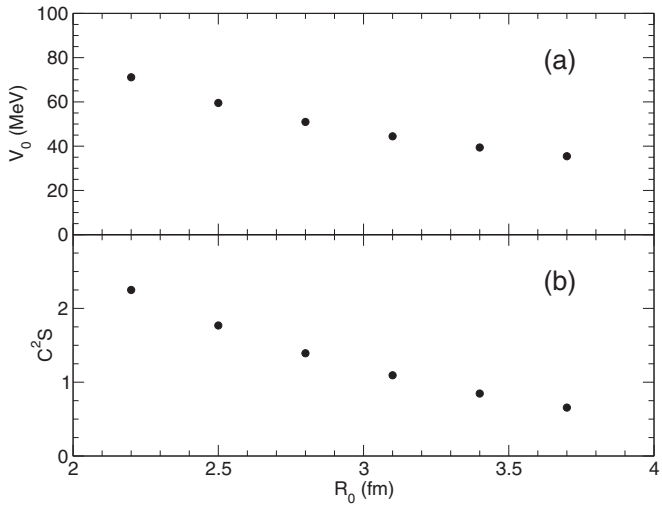

FIG. 10. Values of V_0, R_0 and spectroscopic factors that reproduce the binding energy of the ^{11}B ground state, and provide a satisfactory description of the 1n transfer angular distributions measured at 37.5 MeV.

values found in literature. Concerning the ^{10}B, the $B(E2)$ value found in literature does not reproduce the present experimental data. In order to achieve a satisfactory description of the experimental inelastic-scattering angular distribution for the 1^+ ^{10}B first excited state, we have obtained $B(E2; 3^+ \rightarrow 1^+) = 3.3 \times 10^{-4}$ e^2b^2. Nevertheless, the yield related to this state is very small and the corresponding data could be contaminated by other processes that would lie in the same energy region of the spectra. As ^{10}B is a weakly bound projectile, the effect of couplings to continuum states may play an important role in the description of the reaction mechanisms associated to the nuclear collision. Within this context, a satisfactory description of the experimental inelastic-scattering angular distribution data for the 1^+ ^{10}B first excited state might be achieved using a different $B(E2)$ value.

In order to obtain a reasonable description of elastic- and inelastic-scattering data, we have verified that N_i around 0.25 must be assumed for the imaginary part of the optical potential. The couplings considered in the present work do not have a significant effect, since the theoretical DWBA and CRC calculations result in similar cross sections for all channels. Aiming to improve the agreement between experimental and theoretical angular distributions, probably other channels should be included in the coupling scheme.

For the 1n transfer channel, we could identify two separated groups in the spectra, which correspond to the individual contribution of neighboring states of the compound ^{119}Sn nucleus. The spectroscopic factors for the n + ^{10}B ground state and n + ^{119}Sn ground state and excited states were taken from literature. Adopting a Woods-Saxon binding potential for both neutron-core compound systems, we were able to reproduce satisfactorily the experimental cross sections.

Experimental angular distributions for transfer processes have been extensively used to extract spectroscopic factors from data analyses, which are related to the nuclear structure. Very often, such spectroscopic factors are assumed in data analyses of other works. Nevertheless, in the present case we have demonstrated that is possible to obtain almost identical transfer angular distributions, choosing different sets of parameters for the binding potential in combination with different values for the spectroscopic factors. It is worth mentioning that a particular spectroscopic factor value extracted for one nucleon-core system depends on the binding potentials assumed for both projectile and target compound systems. Therefore, important ambiguities are related to the determination of spectroscopic factor values from data analyses. Indeed, similar results have been reported earlier (e.g., Refs. [32,33]).

ACKNOWLEDGMENTS

This work was partially supported by FAPESP, CNPq, CAPES, and FAPERJ, Brazil, and it is a part of the project INCT-FNA Proc. No. 464898/2014-5.

[1] E. Rutherford, Phil. Mag. **21**, 669 (1911).
[2] I. Tanihata, H. Hamagaki, O. Hashimoto, Y. Shida, N. Yoshikawa, K. Sugimoto, O. Yamakawa, T. Kobayashi, and N. Takahashi, Phys. Rev. Lett. **55**, 2676 (1985).
[3] I. Tanihata, H. Hamagaki, O. Hashimoto, S. Nagamiya, Y. Shida, N. Yoshikawa, O. Yamakawa, K. Sugimoto, T. Kobayashi, D. E. Greiner, N. Takahashi, and Y. Nojiri, Phys. Lett. B **160**, 380 (1985).
[4] P. G. Hansen and B. Jonson, Europhys. Lett. **4**, 409 (1987).
[5] I. Tanihata, H. Savajols, and R. Kanungo, Prog. Part. Nucl. Phys. **68**, 215 (2013).
[6] A. Lépine-Szily, R. Lichtenthaler, and V. Guimarães, Eur. Phys. J. A **50**, 128 (2014).
[7] J. P. Fernández-García, M. Cubero, L. Acosta, M. Alcorta, M. A. G. Alvarez, M. J. G. Borge, L. Buchmann, C. A. Diget, H. A. Falou, B. Fulton *et al.*, Phys. Rev. C **92**, 044608 (2015).
[8] J. J. Kolata, V. Guimarães, and E. F. Aguilera, Eur. Phys. J. A **52**, 123 (2016).
[9] H. Fynbo, O. S. Kirseboom, and O. Tengblad, J. Phys. G **44**, 044005 (2017).
[10] M. Dasgupta *et al.*, Phys. Rev. C **70**, 024606 (2004).
[11] A. Mukherjee *et al.*, Phys. Lett. B **636**, 91 (2006).
[12] P. R. S. Gomes *et al.*, Phys. Rev. C **73**, 064606 (2006).
[13] L. R. Gasques, D. J. Hinde, M. Dasgupta, A. Mukherjee, and R. G. Thomas, Phys. Rev. C **79**, 034605 (2009).
[14] Y. D. Fang *et al.*, Phys. Rev. C **93**, 034615 (2016).
[15] R. Rafiei, R. du Rietz, D. H. Luong, D. J. Hinde, M. Dasgupta, M. Evers, and A. Diaz-Torres, Phys. Rev. C **81**, 024601 (2010).
[16] D. H. Luong, M. Dasgupta, D. J. Hinde, R. du Rietz, R. Rafiei, C. J. Lin, M. Evers, and A. Diaz-Torres, Phys. Lett. B **695**, 105 (2011).

[17] S. Kalkal, E. C. Simpson, D. H. Luong, K. J. Cook, M. Dasgupta, D. J. Hinde, I. P. Carter, D. Y. Jeung, G. Mohanto, C. S. Palshetkar, E. Prasad *et al.*, Phys. Rev. C **93**, 044605 (2016).
[18] G. Baur, C. A. Bertulani, and H. Rebel, Nucl. Phys. A **458**, 188 (1986).
[19] G. Baur and H. Rebel, Annu. Rev. Nucl. Part. Sci. **46**, 321 (1996).
[20] H. Utsunomiya, Y. Tokimoto, H. Mabuchi, K. Osada, T. Yamagata, M. Ohta, Y. Aoki, K. Hirota, K. Ieki, Y. Iwata *et al.*, Phys. Lett. B **416**, 43 (1998).
[21] V. A. B. Zagatto, J. Lubian, L. R. Gasques, M. A. G. Alvarez, L. C. Chamon, J. R. B. Oliveira, J. A. Alcántara-Núñez, N. H. Medina, V. Scarduelli, A. Freitas *et al.*, Phys. Rev. C **95**, 064614 (2017).
[22] L. C. Chamon, B. V. Carlson, L. R. Gasques, D. Pereira, C. DeConti, M. A. G. Alvarez, M. S. Hussein, M. A. Cândido Ribeiro, E. S. Rossi, Jr., and C. P. Silva, Phys. Rev. C **66**, 014610 (2002).
[23] I. J. Thompson, Comp. Phys. Rep. **7**, 167 (1988).
[24] S. Raman, C. W. Nestor, and P. Tikkanen, Atom. Data Nucl. Data Tables **78**, 064615 (2001).
[25] D. F. M. Botero, L. C. Chamon, and B. V. Carlson, J. Phys. G **44**, 105102 (2017).
[26] W. J. Vermeer, R. K. Bhalla, and A. R. Poletti, Phys. Rev. C **28**, 432 (1983).
[27] L. C. Chamon and B. V. Carlson, Nucl. Phys. A **846**, 1 (2010).
[28] O. M. Bilaniuk and J. C. Hensel, Phys. Rev. **120**, 211 (1960).
[29] S. Cohen and D. Kurath, Nucl. Phys. A **101**, 1 (1967).
[30] S. A. Dickey, J. J. Kraushaar, R. A. Ristinen, and M. A. Rumore, Nucl. Phys. A **377**, 137 (1982).
[31] A. J. Koning and J. P. Delaroche, Nucl. Phys. A **713**, 231 (2003).
[32] X. D. Liu, M. A. Famiano, W. G. Lynch, M. B. Tsang, and J. A. Tostevin, Phys. Rev. C **69**, 064313 (2004).
[33] I. J. Thompson and F. M. Nunes, *Nuclear Reactions for Astrophysics: Principles, Calculation and Applications of Low-Energy Reactions* (Cambridge University Press, Cambridge, UK, 2009).